RSC Advances

Continuous detection of trace level concentration of oil droplets in water using microfluidic AC electroosmosis (ACEO)

Journal:	*RSC Advances*
Manuscript ID:	RA-ART-08-2015-015624
Article Type:	Paper
Date Submitted by the Author:	05-Aug-2015

Complete List of Authors:	Das, Dhiman; Nanyang Technological University, School of Chemical and Biomedical Engineering Yan, Zhibin; Nanyang Technological University, School of Mechanical and Aerospace Engineering Menon, Nishanth; Nanyang Technological University, School of Chemical and Biomedical Engineering Kang, Yuejun; Nanyang Technological University, School of Chemical and Biomedical Engineering Chan, Vincent; Nanyang Technological University, School of Chemical and Biomedical Engineering Yang, Chun; Nanyang Technological University, School of Mechanical and Aerospace Engineering

RSC Advances

PAPER

Continuous detection of trace level concentration of oil droplets in water using microfluidic AC electroosmosis (ACEO)

Received 00th January 20xx,
Accepted 00th January 20xx

DOI: 10.1039/x0xx00000x

www.rsc.org/

D. Das,*[ab] Z. Yan,[c] N. V. Menon,[a] Y. Kang,[a] V. Chan,[a] and C. Yang,*[c]

Detection of oil micro-droplets in water is important to environmental oil spill monitoring agencies. We present a microfluidic device for high-throughput trapping oil droplets in water by using an AC electric field in a continuous flow. The electric field is applied through optically transparent indium tin oxide (ITO) electrodes fabricated on a glass substrate to enable direct visualization of the trapped oil droplets in water. The continuously flowing oil droplets in water are trapped by the opposing AC-driven electroosmotic (ACEO) flow due to the formation of electric double layers because of the deposition of polyelectrolytes. The deposition of these polyelectrolytes is necessary for the hydrophilization of the polydimethylsiloxane (PDMS) reactor. An array of SU8 micro-pillars was fabricated within the oil droplet entrapment zone to reduce the hydrodynamic drag force of the incoming fluids. The entrapment efficiency of oil droplets in water was studied as a function of the applied frequency of the electric field. We also observed the presence of a size-dependent negative dielectrophoretic (DEP) force as the droplets exit the entrapment zone. This can improve the entrapment efficiency for larger sized droplets as the strength of the DEP force would be higher.

Introduction

Isolation and detection of micron-sized oil droplets in water is of great importance to environmental oil spillage monitoring applications. Disasters such as the Deepwater Horizon[1] (DWH) oil spill following an explosion in April, 2010 in the Gulf of Mexico remind us about the vulnerability of our ecosystem. It is necessary to break down the floating oil slicks because the marine mammals and seabirds require routine contact with the sea surface[2] and as such oiling of furs and feathers can cause hypothermia, ingestion of toxic hydrocarbons, etc. Thus in the aftermath of such disasters, usually surfactants such as Corexit EC9500A[3] are used to break down the oil slicks which eventually reduce to oil droplets of sizes less than or equal to 70 microns. Oil spill at or near the water surface is also subjected to many physico-chemical processes[4], one of which is the mechanical spreading due to interfacial tension forces, gravity, etc. causing oil slicks on the water surface. The turbulence caused by waves, wind and water currents further break the oil slicks into stable oil-in-water (O/W) emulsions. Owing to a widespread use of such chemicals and external mechanical forces, the micron-sized droplets travel a distance which is very hard to determine accurately via satellites because a substantial portion of the oil is carried by underwater plumes. It was observed after the DWH disaster[1] that more than 212 kilometres of Gulf coastline was moderately to heavily oily by late August, 2010. Currently, fluorescence-based oil detectors [5-7] with detection sensitivity below 1 ppm (parts-per-million) are being used extensively to quantify oil concentration in water. But the major drawback of these detectors is that they are not reliable as the fluorescent signal generated by the instrument does not truly reflect the actual concentration of oil in water[5]. Since the instrument is calibrated using specific oils, the concentration yield which is represented by the fluorescent signal is relative to those specific oils only. Another major disadvantage is that these instruments are bulky, and thus on-field analysis is challenging. Recently, trapping and separation of oil droplets in water was reported by utilizing acoustophoretic force in microfluidic channels etched in silicon wafer [8]. A fluorescent module was incorporated for the optical detection of trapped oil droplets.

In this paper, we present a microfluidic module for the trapping and detection of oil droplets in water by using an alternating current (AC) electric field. When an external AC electric field is applied to an electrolyte contained in microchannels with charged walls, it leads to the formation of an electric double layer (EDL)[9] at the electrolyte-channel wall interface. The EDL can be divided into an inner compact layer and an outer mobile layer[10]. Under the influence of an electric field, the net migration of ions in the outer mobile layer is transmitted to the bulk fluid by viscous forces and regarded as electroosmotic (EO) flow. This kind of fluidic motion has been used to direct electrolytes[10, 11] and referred to as ACEO micropumps. This ACEO phenomenon has also been conveniently used for trapping or concentrating bio-particles around the electrodes[12-15]. In this paper, we use this ACEO phenomenon to

[a] School of Chemical and Biomedical Engineering, Nanyang Technological University, 62 Nanyang Avenue, Singapore-637459.
[b] Nanyang Environment and Water Research Institute, Nanyang Technological University, 1 Cleantech Loop, Singapore-637141.
[c] School of Mechanical and Aerospace Engineering, Nanyang Technological University, 50 Nanyang Avenue, Singapore-639798.

† Electronic supplementary information (ESI) available: Videos and experimental details. See DOI: 10.1039/x0xx00000x

trap the oil droplets around the electrode edges. The electroosmotic flow velocity is given by $U_{eo}=(\varepsilon\varepsilon_0\zeta/\eta).E_t$, where ε is dielectric constant, ε_0 is the permittivity of vacuum, ζ is the surface zeta potential at the electrolyte-charged microchannel wall interface, η is the viscosity of the medium and E_t is the tangential component of the electric field. In other words, U_{eo} is in direct proportion to the amplitude of the applied AC electric field and the strength of the EDL characteristics such as the ζ- potential. But for ACEO, the ζ- potential is not constant as it depends on the applied frequency which determines the rate of polarization of the microchannel and electrolyte interface. It has been reported[16] that at low frequencies, the counterions completely saturates the EDL thereby shielding the EDL from the bulk solution, thus the net flow of the bulk fluid goes to zero. At high frequencies, the counterions do not have enough time to migrate to the rapidly changing charge applied to the electrode surface which affects the formation of the EDL.

In addition to ACEO, applying a non-uniform AC electric field also generates a dielectrophoretic (DEP) force[17, 18] on the bio-particles on account of the difference in polarizability between the particles such as oil droplets and the surrounding aqueous fluid such as water. The time-averaged DEP force[19] is given by

$$\left\langle \vec{F}_{DEP} \right\rangle = 2\pi\varepsilon_m a^3 \,\mathrm{Re}[K(\omega)]\nabla\left|\vec{E}_{rms}\right|^2$$

where $\langle\ \rangle$ represents the time average, ε_m is the permittivity of the medium, *a* is the size of the particle. It is to be noted that the strength of the DEP force increases with increasing size of the particles. $\nabla\left|\vec{E}\right|^2$is gradient of the square of the applied electric field, $\vec{E}_{rms}$ is the root-mean square electric field, Re[K(**ω**)]=Re[($\underline{\varepsilon}_p$-$\underline{\varepsilon}_m$)/($\underline{\varepsilon}_p$+2$\underline{\varepsilon}_m$)] is the real part of the Clausius-Mossotti(CM) or polarization factor ranging from -0.5 to 1, $\underline{\varepsilon}$=ε-i (σ/ω) is the complex permittivity with σ as electrical conductivity, $i=\sqrt{-1}$, ω=2**p**f is the frequency of the applied electric field. $\underline{\varepsilon}_p$ is the permittivity of the particle, $\underline{\varepsilon}_m$ is the permittivity of the medium. Depending on whether the bio-particles are more or less polarizable than the surrounding fluid, they tend to move towards or away from the high intensity electric field zone and henceforth, the DEP force is classified as positive, p-DEP(such that Re[K(**ω**)]>0) or negative, n-DEP(such that Re[K(**ω**)]<0), respectively. The present study utilizes the fact that as oil droplets are less conductive than water, it will be repelled by the high electric field zones. Several n-DEP force-based traps[20] have been reported for concentrating generic particles like latex[21] and polystyrene[22] beads, cells like escherichia coli[23], yeast[24] and so forth.

Due to hydrophobic nature of PDMS, oil droplets usually stick to native PDMS walls and eventually clog the microchannels. Hence, a surface treatment step[25] is incorporated. Thereafter, experiments are performed to study the effect of frequency on electroosmosis via its trapping efficiency. In our experiments, we also observe the fusion of oil droplets to attain a larger size in the entrapment zone and that there is an increase in the linear velocity for the larger sized droplets as they exit the entrapment zone. This confirms the presence of a size dependent DEP force which implies that the entrapment efficiency would be enhanced for larger sized droplets.

Experimental

Microchip Fabrication

A schematic of the microfluidic device is shown in Fig. 1(a). First, a 0.7-mm thick glass coated with a conductive indium tin oxide (ITO) (Optoelectron Technologies, Singapore) film was taken as the base plate of the microfluidic device. ITO was chosen as it is optically transparent and enables us to visualize the droplets through the electrodes as the droplets are trapped over the electrodes due to the ACEO flow field. The ITO patterns on glass were obtained by using AZ photoresist followed by acid etching in HCl: H_2O: HNO_3 (4:2:1 by volume) solution to obtain an electrode gap of 310 microns. Thereafter, SU8 micro-pillars of 10 microns height, was obtained by spincoating followed by UV exposure over the ITO patterned glass substrate. PDMS blocks were then placed over the micro-pillars on the ITO etched base glass plate after plasma treatment.

The width and height of the microchannels is 40 microns whereas the diameter of the circular shaped oil droplet entrapment zone is 800 microns as shown in Fig. 1(b). Then hydrophilization of the PDMS-glass substrate microchannels was through (LbL) deposition scheme of alternately charged polyelectrolyte solutions poly(allylamine hydrochloride) (PAH) (Sigma, Singapore) and negatively charged poly(sodium 4-styrenesulfonte) (PSS) (Sigma, Singapore) by flushing it in the sequence PAH-PSS-PAH-PSS[25] immediately after plasma treatment. This renders the microchannel surface negatively charged which was followed by flushing the microchannels with Triton X-100 at critical micelle concentration (CMC) in order to remove the loosely attached ions from the microchannel walls.

Experimental set-up

Two syringe pumps (KD Scientific) with 0.5 ml Hamilton glass syringes are used for pushing the two immiscible fluids: dispersed phase, oil and the continuous phase, water. The droplet trapping at the circular zone of the microchip is observed with a Carl Zeiss microscope fitted with a Zeiss lens (CP-Achromat 5x/0.12) and a Phantom Miro M310 digital high-speed camera at 200 frames per second. A function generator (Agilent 33250A) is connected with an amplifier (AVC 790 Series Power Amplifier) by a BNC cable to produce AC voltages of desired frequencies which is imposed on the ITO electrodes.

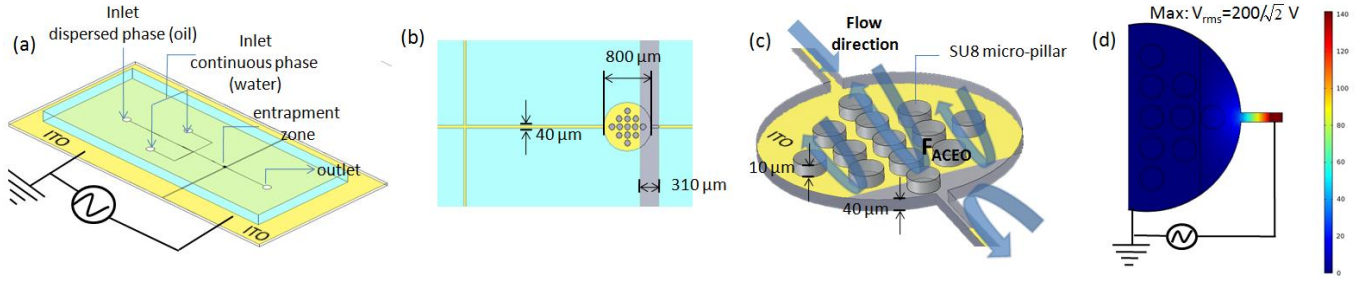

Fig.1 (a) Schematic illustration of the microchip showing the inlets for dispersed phase, oil and continuous phase, water; the entrapment zone and the ITO electrodes over the base glass substrate (b)Dimensions of the microchannels(both width and height is 40 µm), entrapment zone(800 µm) and the electrode gap(310 µm) (c) Droplet entrapment zone with the counter-rotating vortices emerging from the parallel ITO electrodes and the SU8 micro-pillar array of height 10 µm and diameter 100 µm each (not drawn according to scale) (d) Electric potential (V) at an applied AC voltage of 200 Vp-2-p at the outlet of the entrapment zone obtained from Comsol Multiphysics 4.4.

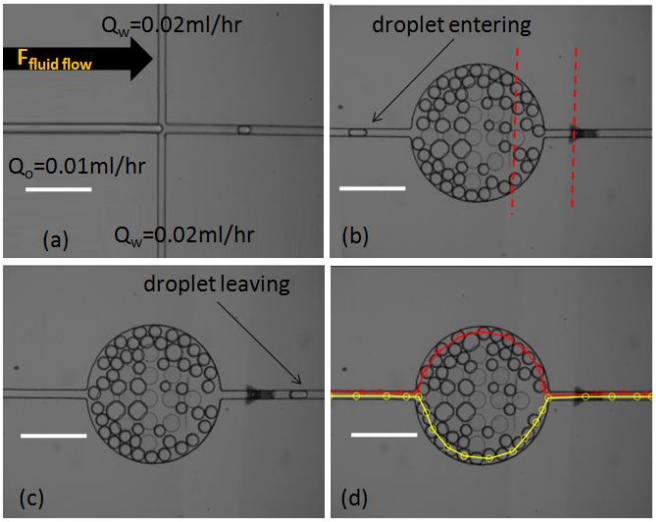

Fig.2 (a) Cross-flow junction for generation of oil droplets where Q_o and Q_w are the volumetric flow rates of oil and water, respectively. (b) a droplet entering the trapping structure and the highlighted red lines are electrode edges towards the outlet. (c) a droplet exiting the trapping structure. (d) trajectory of the droplets around the SU8 micropillar array. Scale bars denote 400 µm.

Oil droplet generation

Silicone oil (Sigma, Singapore) of viscosity 50 cSt was used as the dispersed phase. The oil phase was then emulsified into discrete droplets in an aqueous and immiscible non-ionic surfactant Triton X-100 (Bio-Rad Laboratories, Singapore) solution at the critical micelle concentration value, which makes up the continuous and immiscible aqueous phase. We used a cross flow junction for the emulsification of dispersed phase consisting of silicone oil (50 cSt, density=960 kg/m^3) into individual droplets as shown in Fig.2(a). We did not use ionic surfactants because they might lead to rapid oxidation, darkening and degradation of the ITO electrodes and gas formation at both electrodes at high voltages due to their higher conductivity. The dispersed oil phase was sheared off by the continuous water phase. The initial size of the oil droplets was slightly bigger before the flow was fully stabilized. Gradually over time, the size of the droplets became more consistent. In our experiments, we kept the dispersed oil phase flow rate at 0.01 ml/hr and continuous phase water flow rate at 0.04 ml/hr to have a consistent droplet size.

Results and discussion

Micro-pillar array and oil droplet trapping

Trapping of oil droplets is achieved in a circular shaped oil droplet enrichment zone which contains the micro-pillar array. Initially, the gap between the micro-pillars was filled with droplets. These droplets become immobilized and together with micro-pillars offer the hydrodynamic resistance which is necessary to slow down the incoming oil droplets. Finally, equilibrium is achieved such that a finite volume of oil droplets is maintained in the circular oil enrichment zone as the rate of the incoming droplets is equal to the rate of droplets exiting the enrichment zone. Fig. 2 (b) and (c) shows two images of oil droplets as one enters the entrapment zone, another exits the same. The trajectory of the oil droplets is shown in Fig. 2(d) which indicates that the oil droplets make its way around the micro-pillars. To prevent the escaping of droplets from the enrichment zone, an electric field is imposed. Two ITO electrodes are positioned in such a way that the escaping droplets will have to go over the electrode gap at the outlet from the circular shaped entrapment chamber. We chose this electrode design because it is motivated by the ACEO flow field experiments[12, 13] around the planar electrodes where the particles are pushed away from the electrode gap. Hence, our device is designed in such a way that the droplets would have to go over the electrode gap to escape from the entrapment zone. Due to the constriction of the circular shaped entrapment shape, a non-uniform electric field is generated and the strength of the normalized electric field (V/m) is highest at the outlet where the droplets are trapped (Fig.3). When the applied AC signal was 200 V and 100 Hz, the trapping efficiency in the entrapment zone was increased by up to 47.6% (Fig.4), which finally became saturated and caused oil droplets to leak after the oil concentration exceeded the threshold limit.

Considering that the smallest size of the oil droplet which was trapped in the circular entrapment zone has a diameter of 40 microns at a total aqueous flow rate of 0.04 ml/hr for the external water phase, the detection limit of the microfluidic device was

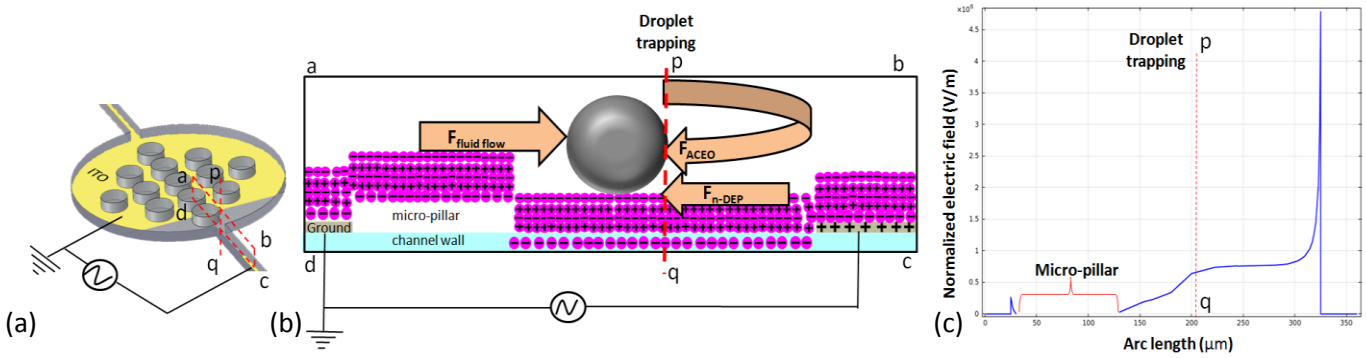

Fig.3 (a) the cut-plane abcd at the outlet. The droplets are trapped in the cut-line pq.(b) the physical forces acting on an oil droplet inside the cut-plane abcd when it gets trapped at pq. [Charged ions in the purple circles illustrate a schematic of the LbL surface modification of a PDMS-glass microchannel using PAH (positive) and PSS (negative) polyelectrolyte solutions. The negatively charged channel wall and over the micro-pillar is due to plasma treatment.] (c) Normalized electric field (V/m) along the cut-line dc at the bottom of the microchannel. pq shows the increase in electric field strength obtained from Comsol Multiphysics 4.4 where the droplets are trapped.

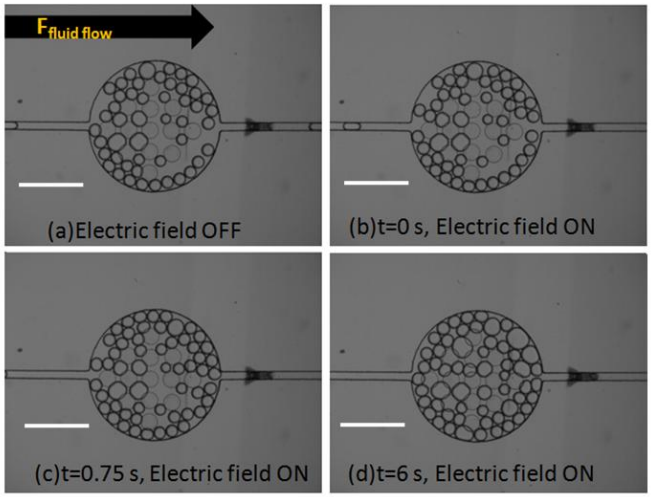

Fig.4 (a), (b), (c), (d) the trapping of the oil droplets over time under an AC electric field of 200 V and 100 Hz is applied. Scale bars denote 400 µm.

about 3.22 ppm when the system was continuously running for a duration of 15 min. This detection limit can be further improved by increasing the size of the circular entrapment zone and also by running several devices in parallel which will compensate for more volume of the processed fluids for the same duration of time.

Entrapment efficiency measurement

Initially, videos were obtained to capture the passage of oil droplets through the enrichment zone using a digital high-speed camera, Phantom Miro M310 at a rate of 200 frames per second.

Thereafter, snapshots were taken at a specific time intervals. This was followed by counting the pixels within the oil droplets using an open source image processing program, ImageJ (National Institutes of Health, USA). A detailed explanation is given in the supplementary note. In the absence of electric field, there is a balance between the rate of incoming droplets and the rate of outgoing droplets in the enrichment zone and thus the total volume of droplets stays the same. This is reflected in Fig. [2(b) and (c)] where the total pixel count within the droplets stays constant versus time as long as no applied electric field . When the electric field is turned on, the number of droplets trapped in the enrichment zone increases as seen in Fig. 4 until the hydrodynamic drag force in the entrapment zone is able to overcome the n-DEP force and ACEO flow field. This is reflected in the increase of pixel count within the droplets, when the electric field is turned on, which eventually becomes stable. We used the ratio of total number of pixels within the oil droplets before and after the electric field was applied to quantify the effect of the applied electric field on the entrapment efficiency.

DEP force and ACEO flow field for oil droplets entrapment

Since the dielectric permittivity of oil (ε_{oil} = 2.5) is much lower than that of water (ε_{water} = 80)[26], the presence of a negative DEP force will repel the oil droplets from the high electric field zone at the outlet. Hence, the oil droplets would be trapped. It was reported that silicone oil has a virtually constant electrical conductivity ~ 10^{-13} Sm^{-1} [27] regardless of the electrical field applied. Taking the electrical conductivity of DI water as 5.5 mS/m , we can obtain the values of the real part of the CM factor using the expression[28]

$$\mathrm{Re}[K(\omega)] = \frac{\omega^2(\varepsilon_p - \varepsilon_m)(\varepsilon_p + 2\varepsilon_m) + (\sigma_p - \sigma_m)(\sigma_p + 2\sigma_m)}{\omega^2(\varepsilon_p + 2\varepsilon_m)^2 + (\sigma_p + 2\sigma_m)^2}$$

and obtain that Re[K(**ω**)] stays constant at approximately at -0.47 from 0 to 100 kHz. Here, ε_p and ε_m denote the dielectric permittivity of oil droplets and DI water, respectively. Hence, a change in the frequency of the applied AC electric field does not affect the strength of the DEP force, provided that the size of the droplets remains the same. However, that fusion of droplets was observed as they were trapped between the micro-pillars and they were pushed forward by the fluidic motion from behind and back by the combined n-DEP and ACEO flow field upon activation of the electric field. In Fig. 5(a, b), we present the linear velocity of the droplets as the rear end of the droplets goes over the electrode edge at the outlet to confirm the presence of n-DEP force as it acts both

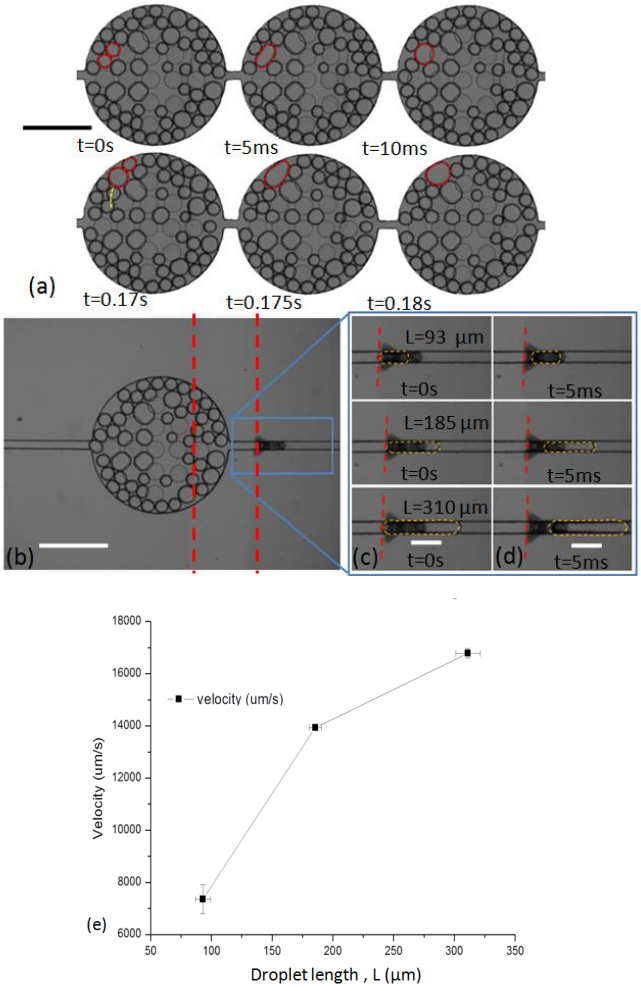

Fig.5 (a) the fusion of three oil droplets over time. The droplets which fuse are highlighted in red. The first two droplets fuse at t= 0.005 s. At t= 0.17s, we have shown the trajectory of the droplets in yellow, thereafter which it fuses again at t=0.175 s;(b) exit channel from the entrapment zone and (c) shows inset figure of the same for three different droplet lengths, L=93 µm (obtained from the cross-flow junction used for droplet generation), 185 µm (obtained from the fusion of two droplets) and 310 µm (obtained from the fusion of three droplets) as the rear-end of the droplet over the electrode edge shown in dashed red line after it has exited the entrapment zone, (d) shows the position of the same three droplet after 0.005 s ;(e) shows the effect of the droplet length, L on the linear velocity of the same as it goes past the electrode edge obtained from the images as shown in(c) and (d). Scale bars denote 400 µm in(a),(b) and 100 µm in(c),(d).

towards and away from the electrode edge. This is because there is a high electric field at the electrode edge which will repel the oil droplets. The Phantom Camera Control (PCC 2.14b) software was used to analyze the videos in order to determine the exact velocity of the droplets. The different sizes of droplets are obtained from the fusion of the smaller droplets around the micro-pillars in the circular shaped entrapment zone. Droplets of length 90 to 100 microns were obtained using dispersed oil phase flow rate at 0.01 droplet of length varying between 310 to 320 microns. The fusion of the droplets is shown in Fig. 5 (a). It can be concluded that as the size of the droplets increases, the velocity of the droplets moving past the electrode edge also increases accordingly as shown in Fig. 5 (d), which confirms the presence of the size-dependent n-DEP force. This may have profound effect on the entrapment efficiency of the microfluidic reactor if it is used to trap larger sized droplets because the strength of the n-DEP force would be enhanced.

A 200 Vp-p was applied for a range of frequencies to observe the AC frequency effect on the entrapment efficiency. It was observed that switching the electrodes for reversing the polarity of the applied electric field made no difference to the entrapment efficiency. A possible explanation maybe that the ACEO flow field created by the counter-rotating vortices[12, 13] due to the electric field distribution above the planar ITO electrodes, is independent of direction of the applied electric field. Oscillation of the droplets at large distances from the electrode gap also confirms the presence of strong ACEO flow. Because the electroosmotic force depends on EDL characteristics such as the ζ- potential and is not size-dependent, this design can be used to trap oil droplet with a wide range of sizes. For all frequencies from 10^0 to 10^4 Hz, we noticed that the droplets were immediately trapped after the electrode field was turned on. At low frequencies, the droplets were only trapped for the first half cycle when the AC field was positive. When the electric field changed direction in the second half of the AC cycle, the ions generated from the electrochemical reactions were consumed by the reverse reactions, which reduced the net ACEO flow and caused the droplets to be released due to the incoming hydrodynamic drag force of the bulk electrolyte solution.

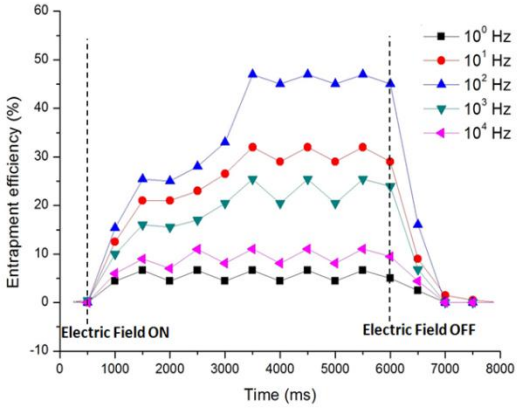

Fig.6 Entrapment efficiency of the device obtained as a function of frequency at 200 Vp2p. The electric field is turned on at 500 ms and turned off at 6000 ms.

The experimental results (Fig. 6) exhibits the lowest entrapment efficiency at 1 Hz. The entrapment efficiency increases considerably at 10 Hz and is further increased to the maximum under 100 Hz. Beyond 100 Hz, the entrapment efficiency decreases as the rate of electrode polarization is too fast to form the EDL, thereby weakening the generated ACEO flow field. Hence, the results suggest that an applied voltage at 100 Hz provides the optimum oscillation frequency, under which the electrode polarization time scale is comparable to the charge relaxation time scale of the EDL obtained from the hydrophilization coating schemes.

We also observe that it is imperative to flush the microchannels with a non-ionic surfactant for about 45 min prior to switching on the electric field because the presence of loosely attached polyelectrolyte ions can result in a large current density passing through the electrolyte. This causes rapid degradation of the ITO film in high electric field regions when the oxides in ITO are reduced. For example, In_2O_3 and SnO_2 are reduced to Indium, In and Tin, Sn and the evolved oxygen generates bubbles[29]. The evolved metal ions of In and Sn then migrate under the influence of electric field and cause darkening of the electrodes. It must be noted that real-time marine samples are saline and as such will lead to reduction of the ITO electrodes. Hence, the saline water may be diluted to reduce the ionic conductivity of the working fluid, however that would reduce the throughput of the device. A suitable alternative to ITO electrodes may be carbon-paste electrodes [30, 31] as they are more resistant to fouling and can withstand a wider potential range. This work is significant in determining the electrode and microchannel configuration needed for trapping oil droplets in water and hence can be considered useful for designing fully automatic schemes in the future.

Conclusion

This work reported a new microfluidic device for continuous detection of oil droplets in water. A PDMS and ITO glass based microchip was developed to continuously trap oil droplets from DI water by AC electroosmosis. The micro-pillars were used to reduce the hydrodynamic drag force on the incoming oil droplets. Since PDMS is inherently hydrophobic, we applied the LbL surface modification technique that rendered negatively charged and hydrophilic PDMS and glass surfaces contributing to a strong ACEO flow field for oil droplet trapping. Experiments were performed at an appropriate frequency range for analyzing the entrapment efficiency for our device. It was demonstrated that highest entrapment efficiency obtained was 47.6% at an applied voltage and frequency of 200 Vp-p and 100 Hz, respectively. Furthermore, we observed the fusion of oil droplets in the entrapment zone and the presence of a size-dependent DEP force. It was noted that the linear velocity of the droplets increased with size as the droplets exited the entrapment zone and moved over the electrode edge. These results suggested that the entrapment efficiency could be further enhanced for larger sized droplets.

Acknowledgements

The first author gratefully acknowledges the postgraduate student scholarship from NEWRI, Singapore which is supported by Singapore National Research Foundation under its Environmental & Water Technologies Strategic Research Programme and administered by the Environment & Water

Industry Programme Office (EWI) of the PUB. Y.K. gratefully acknowledges the Tier 2 Academic Research Fund (ARC 22/13) and Tier 1 Academic Research Fund (RG 37/14) from the Ministry of Education of Singapore.

References

1 (1)Mascarelli, A. (2010) Deepwater Horizon: After the oil. *Nature*, 467: 22.

2 (2)Peterson, C.H.; Rice, S.D.; Short, J.W.; Esler, D.; Bodkin, J.L.; Ballachey, B.E.; Irons, D.B. (2003) Long-Term Ecosystem Response to the Exxon Valdez Oil Spill. *Science*, 302(5653): 2082-2086.

3 (3)Mendoza, W.G.; Riemer, D.D.; Zika, R.G. (2013) Application of fluorescence and PARAFAC to assess vertical distribution of subsurface hydrocarbons and dispersant during the Deepwater Horizon oil spill. *Environmental Science: Processes & Impacts*, 15(5): 1017-1030.

4 (4)Handbook of Environmental Fluid Dynamics : Systems, Pollution, Modeling, and Measurements. In Fernando, H.J., Ed. CRC Press: December 12, 2012; Vol. Volume Two, p 587.

5 (5)Lambert, P.; Goldthorp, M.; Fieldhouse, B.; Wang, Z.; Fingas, M.; Pearson, L.; Collazzi, E. (2003) Field fluorometers as dispersed oil-in-water monitors. *Journal of Hazardous Materials*, 102(1): 57-79.

6 (6)Lambert, P. (2003) A literature review of portable fluorescence-based oil-in-water monitors. *Journal of Hazardous Materials*, 102(1): 39-55.

7 (7)Kim, M.; Yim, U.H.; Hong, S.H.; Jung, J.-H.; Choi, H.-W.; An, J.; Won, J.; Shim, W.J. (2010) Hebei Spirit oil spill monitored on site by fluorometric detection of residual oil in coastal waters off Taean, Korea. *Marine Pollution Bulletin*, 60(3): 383-389.

8 (8)Wang, H.; Liu, Z.; Kim, S.; Koo, C.; Cho, Y.; Jang, D.-Y.; Kim, Y.-J.; Han, A. (2014) Microfluidic acoustophoretic force based low-concentration oil separation and detection from the environment. *Lab on a Chip*, 14(5): 947-956.

9 (9)Hunter, R.J. (1981) COLLOID SCIENCE *Zeta Potential in Colloid Science*;Academic Press:New York

10 (10)Yang, C. (2002) Transport of Liquid in Rectangular Microchannels by Electroosmotic Pumping in Tay, F.H. (Ed) *Microfluidics and BioMEMS Applications*;Springer US

11 (11)Chuan-Hua, C.; Santiago, J.G. (2002) A planar electroosmotic micropump. *Microelectromechanical Systems, Journal of*, 11(6): 672-683.

12 (12)Wu, J.; Ben, Y.; Battigelli, D.; Chang, H.-C. (2005) Long-Range AC Electroosmotic Trapping and Detection of Bioparticles. *Industrial & Engineering Chemistry Research*, 44(8): 2815-2822.

13 (13)Islam, N.; Wu, J. (2006) Microfluidic transport by AC electroosmosis. *International MEMS Conference, Journal of Physics: Conference Series* 34.

14 (14)Pak Kin, W.; Che-Yang, C.; Tza-Huei, W.; Chih-Ming, H., An AC electroosmotic processor for biomolecules. In *TRANSDUCERS, Solid-State Sensors, Actuators and Microsystems, 12th International Conference on, 2003*, 2003; Vol. 1, pp 20-23 vol.21.

15 (15)Bown, M.R.; Meinhart, C.D. (2006) AC electroosmotic flow in a DNA concentrator. *Microfluidics and Nanofluidics*, 2(6): 513-523.

16 (16)Gagnon, Z.; Chang, H.C. (2005) Aligning fast alternating current electroosmotic flow fields and characteristic frequencies with dielectrophoretic traps to achieve rapid bacteria detection. *Electrophoresis*, 26(19): 3725-3737.

17 (17)Pohl, H.A. (1978) *Dielectrophoresis- The Behaviour of Neutral Matter in Nonuniform Electric Fields*;Cambridge University Press Cambridge(UK)

18 (18)Denner, V.; Pohl, H.A. (1982) Dielectrophoretic force in electrostatic fields. *Journal of Electrostatics*, 13(2): 167-174.

19 (19)Lewpiriyawong, N.; Yang, C.; Lam, Y.C. (2010) Continuous sorting and separation of microparticles by size using AC dielectrophoresis in a PDMS microfluidic device with 3-D conducting PDMS composite electrodes. *Electrophoresis*, 31(15): 2622-2631.

20 (20)Nilsson, J.; Evander, M.; Hammarström, B.; Laurell, T. (2009) Review of cell and particle trapping in microfluidic systems. *Analytica Chimica Acta*, 649(2): 141-157.

21 (21)Thomas, R.S.; Morgan, H.; Green, N.G. (2009) Negative DEP traps for single cell immobilisation. *Lab Chip*, 9(11): 1534-1540.

22 (22)Rosenthal, A.; Voldman, J., Simple, Strong, size-selective dielectrophoretic traps for single-cell patterning. In *Micro-Total Analysis Systems 2004, Proceedings of uTAS 2004*, Royal Society of Chemistry, Cambridge: Malmo, Sweden, 2004; Vol. 2, pp 228-230.

23 (23)Donato, S.S.; Chu, V.; Prazeres, D.M.; Conde, J.P. (2013) Metabolic viability of Escherichia coli trapped by dielectrophoresis in microfluidics. *Electrophoresis*, 34(4): 575-582.

24 (24)Wang, X.B.; Huang, Y.; Burt, J.P.H.; Markx, G.H.; Pethig, R. (1993) Selective dielectrophoretic confinement of bioparticles in potential energy wells. *Journal of Physics D: Applied Physics*, 26(8): 1278.

25 (25)Bauer, W.-A.C.; Fischlechner, M.; Abell, C.; Huck, W.T.S. (2010) Hydrophilic PDMS microchannels for high-throughput formation of oil-in-water microdroplets and water-in-oil-in-water double emulsions. *Lab on a Chip*, 10(14): 1814-1819.

26 (26)Wang, W.; Yang, C.; Li, C.M. (2009) On-demand microfluidic droplet trapping and fusion for on-chip static droplet assays. *Lab Chip*, 9(11): 1504.

27 (27)ZHANG, H.B.; EDIRISINGHE, M.J.; JAYASINGHE, S.N. (2006) Flow behaviour of dielectric liquids in an electric field. *Journal of Fluid Mechanics*, 558: 103-111.

28 (28)Nuttawut, L., Continuous separation and manipulation of particles and cells using dielectrophoresis. . In Nanyang Technological University, Singapore: 2011; Vol. Phd Thesis.

29 (29)He, J.; Lu, M.; Zhou, X.; Cao, J.R.; Wang, K.L.; Liao, L.S.; Deng, Z.B.; Ding, X.M.; Hou, X.Y.; Lee, S.T. (2000) Damage study of ITO under high electric field. *Thin Solid Films*, 363(1–2): 240-243.

30 (30)Sameenoi, Y.; Mensack, M.M.; Boonsong, K.; Ewing, R.; Dungchai, W.; Chailapakul, O.; Cropek, D.M.; Henry, C.S. (2011) Poly(dimethylsiloxane) cross-linked carbon paste electrodes for

microfluidic electrochemical sensing. *Analyst*, 136(15): 3177-3184.
31 (31)Suea-Ngam, A.; Rattanarat, P.; Chailapakul, O.; Srisa-Art, M. (2015) Electrochemical droplet-based microfluidics using chip-based carbon paste electrodes for high-throughput analysis in pharmaceutical applications. *Analytica Chimica Acta*, 883: 45-54.
32